arXiv:1703.02336v2 [cs.SY] 9 Mar 2017

A scalable line-independent design algorithm for voltage and frequency control in AC islanded microgrids

Michele Tucci*[1] and Giancarlo Ferrari-Trecate†[2]

[1] *Dipartimento di Ingegneria Industriale e dell'Informazione, Università degli Studi di Pavia, Italy*

[3] *Automatic Control Laboratory, École Polytechnique Fédérale de Lausanne (EPFL), Switzerland*

Technical Report
March, 2017

Abstract

We propose a decentralized control synthesis procedure for stabilizing voltage and frequency in AC Islanded microGrids (ImGs), i.e. electrical networks composed of interconnected Distributed Generation Units (DGUs), power lines and loads. The presented approach enables Plug-and-Play (PnP) operations, meaning that DGUs can be arbitrarily added or removed without compromising the overall ImG stability. The main feature of our approach is that, differently from [1], the proposed PnP design algorithm is line-independent. This implies that (i) the synthesis of each local controller does not require anymore the model of power lines connecting neighboring DGUs, and (ii) whenever a new DGU is plugged-in, DGUs physically connected to it do not have to retune their regulators. Theoretical results are validated by simulating in PSCAD the behavior of a 10-DGUs ImG.

Keywords: Distributed control, voltage and frequency control, asymptotic stability, electrical networks, renewable energy systems.

*Electronic address: michele.tucci02@universitadipavia.it; Corresponding author
†Electronic address: giancarlo.ferraritrecate@epfl.ch

1 Introduction

Voltage and frequency stability is a central problem in low-voltage AC Islanded microGrids (ImGs) and, in the recent years, it has received great attention within the Control and the Power Electronics communities [2]. In absence of a connection to the main grid (which acts as an infinite power source) and a master clock for the ImG frequency, voltage and frequency must be governed by the local controllers of the Voltage Source Converters (VSCs) interfacing power sources with the ImG. Each controlled VSC, together with its power supply, forms a Distributed Generation Unit (DGU) connected to loads and other DGUs through power lines. Voltage and frequency control can be then formulated as the problem of designing decentralized regulators which are stabilizing in spite of the electrical coupling between DGUs. Approaches to the decentralized control of ImGs can be divided into two main classes. The first one embraces droop controllers [2], which mimic standard regulators for power networks with inertial generators. Droop controllers admit a simple implementation and do not require synchronized clocks for the computation of the control signals. However, they can generate frequency drifts, whose compensation calls for the use of secondary distributed controllers [2]. Stability properties of droop-controlled microgrids have been analyzed in [3, 4] under simplified models of the DGU dynamics. The second class of controllers comprises solutions based on approaches developed within the field of decentralized control [5, 6, 7, 8, 1]. If, on the one hand, they require controller clocks to be synchronized with sufficient precision (through, e.g., GPS or communication networks [9]), on the other hand, they enjoy built-in stability and robustness properties.

Control design algorithms for ImGs can be also categorized according to their level of modularity. In order to enable the deployment of mGs with flexible structure [10], where DGUs and loads can enter/leave over time, one needs a control architecture that can be easily updated when the ImG topology changes. Approaches of this kind have been often termed Plug-and-Play (PnP) [11, 12, 1, 13, 14]. In particular, in [1], PnP means that (i) the computation of a local controller for a DGU requires only models of power lines connected to it, and (ii) the design of a local controller preserving voltage and frequency stability in the whole ImG amounts to an optimization problem. Note that, in view of (i), no global model of the ImG is needed in control design. Moreover, the plug-in of a DGU requires to update controllers of neighboring DGUs, at most. In addition, from (ii), the plug-in of a DGU can be automatically denied if stabilizing controllers for the DGU and its neighbors cannot be found. Approaches to the design of distributed regulators with similar PnP features for large-scale systems have been proposed in [15, 16, 17, 18].

In this paper we develop a PnP control design method that, differently from [1] does not require knowledge of power lines. This simplification is desirable for two main reasons. First, the addition/removal of a DGU does not require to update any existing controller in the ImG. Indeed, plugging-in/out operations do affect the lines connected to neighboring DGUs, but DGU controllers are line-independent. Second, control design does not require line parameters, which are often uncertain. In addition, PnP design in [1] was dependent on a global tuning parameter (which had to be sufficiently small), while here this constraint is removed. Rather, we exploit the fact that DGU interactions can be represented through the Laplacian matrix of the electric graph for guaranteeing the decrease of a separable Lyapunov function along state trajectories. This, together with the application of the LaSalle invariance principle, allows us to prove voltage and frequency stability in the whole ImG.

The approach taken in this paper share several similarities with the one in [19], where DC mGs are considered and a line-independent variant of the PnP design algorithm in [12] has been proposed. There is, however, a fundamental difference: in the AC case, one must handle three-phase balanced signals or, in an equivalent way, their dq representation (see, e.g., [20]). Besides making the proofs more involved, this impacts on the optimization problems that have to be solved for the design of local controllers. Indeed, differently from [19], Linear Matrix Inequality (LMI) constraints are not sufficient for guaranteeing stability and they must be complemented with nonlinear constraints.

The paper is structured as follows. The ImG model is presented in Section 2. Section 3 describes the procedure for designing PnP controllers and the stability analysis of the closed-loop

ImG. Simulation results using a 10-DGU ImG with linear and nonlinear loads are shown in Section 4.

Notation and basic definitions. The N-dimensional identity and null matrix are denoted, respectively, with I_N and $\mathbf{0}_N$, while we use $\mathbf{0}$ to indicate a null matrix of appropriate size. Let $A \in \mathbb{R}^{n\times m}$ be a matrix inducing the linear map $A : \mathbb{R}^m \to \mathbb{R}^n$. The *image* and the *nullspace* (or *kernel*) of A are indicated with $\mathrm{Im}(A)$ and $\mathrm{Ker}(A)$, respectively. Consider the subspace $B \subseteq \mathbb{R}^m$: with $A\big|_B$ we denote the restriction of the map A to the domain B. The symbol $\oplus$ refers to the sum of subspaces that are orthogonal (also called *orthogonal direct sum*).

2 Microgrid model

In this section, we present the electrical model of the ImG we used. We assume three-phase electrical signals without zero-sequence components and balanced network parameters (see [20] for basic definitions about AC three-phase signals).

The single-phase equivalent scheme of DGU i is shown in the dashed frame of Figure 1. In particular, we have a DC voltage source for modeling a generic renewable resource and a VSC is controlled in order to supply a local load, connected to the Point of Common Coupling (PCC) through an *RLC* filter. Notice that, by considering only loads connected at the PCC of each DGU, we do not loose generality. In fact, as shown in [21, 22], general interconnections of loads and DGUs can always be mapped into this topology by means of a network reduction method known as Kron reduction. We further assume that loads I_{Li} are unknown and act as current disturbances [7].

More in general, we can consider an ImG composed of N DGUs and define the set $\mathcal{D} = \{1, \dots, N\}$. Then, we (i) call two DGUs neighbors if there is a power line connecting their PCCs, (ii) denote with $\mathcal{N}_i \subset \mathcal{D}$ the subset of neighbors of DGU i, and (iii) observe that the neighboring relation is symmetric (i.e. $j \in \mathcal{N}_i$ implies $i \in \mathcal{N}_j$). We denote with $\mathcal{G}_{el}$ the undirected electric graph induced by the neighboring relation over the node set $\mathcal{D}$. Let ω_0 be the reference network frequency. As in [1, 22], the DGU model in dq reference frame (rotating with speed ω_0) is

$$\text{DGU } i: \quad \begin{cases} \dfrac{\mathrm{d}}{\mathrm{d}t} V_i^{dq} = -\mathrm{i}\omega_0 V_i^{dq} + \dfrac{I_{ti}^{dq}}{C_{ti}} - \dfrac{I_{Li}^{dq}}{C_{ti}} + \displaystyle\sum_{j\in\mathcal{N}_i} \frac{1}{C_{ti}} \left(\frac{V_j^{dq}}{R_{ij} + \mathrm{i}\omega_0 L_{ij}} - \frac{V_i^{dq}}{R_{ij} + \mathrm{i}\omega_0 L_{ij}} \right) \\ \dfrac{\mathrm{d}}{\mathrm{d}t} I_i^{dq} = -\left(\dfrac{R_{ti}}{L_{ti}} + \mathrm{i}\omega_0 \right) I_{ti}^{dq} - \dfrac{V_i^{dq}}{L_{ti}} + \dfrac{V_{ti}^{dq}}{L_{ti}} \end{cases} \tag{1}$$

where quantities V_i^{dq} and I_{ti}^{dq}, represent the i-th PCC voltage and filter current, respectively, V_{ti}^{dq} is the command input to the corresponding VSC, while R_{ti}, L_{ti} and C_{ti} are the converter parameters. Moreover, V_j^{dq} is the voltage at the PCC of each neighboring DGU $j \in \mathcal{N}_i$ and R_{ij} and L_{ij} are, respectively, the resistance and impedance of the three-phase power line connecting DGUs i and j. Moreover, we recall that (1) has been derived by exploiting QSL approximation of power lines [1].

2.1 ImG state-space model

In this section, we derive the state-space model of the ImG with dynamics (1). Notably, we can write

$$\Sigma_{[i]}^{DGU}: \begin{cases} \dot{x}_{[i]}(t) = A_{ii} x_{[i]}(t) + B_i u_{[i]}(t) + M_i d_{[i]}(t) + \xi_{[i]}(t) \\ y_{[i]}(t) = C_i x_{[i]}(t) \\ z_{[i]}(t) = H_i y_{[i]}(t) \end{cases} \tag{2}$$

where $x_{[i]} = [V_i^d, V_i^q, I_{ti}^d, I_{ti}^q]^T$ is the state, $u_{[i]} = [V_{ti}^d, V_{ti}^{q]^T}$ the control input, $d_{[i]} = [I_{Li}^d, I_{Li}^q]^T$ the exogenous input and $z_{[i]} = [V_i^d, V_i^q]^T$ the controlled variable of the system. Moreover, we assume

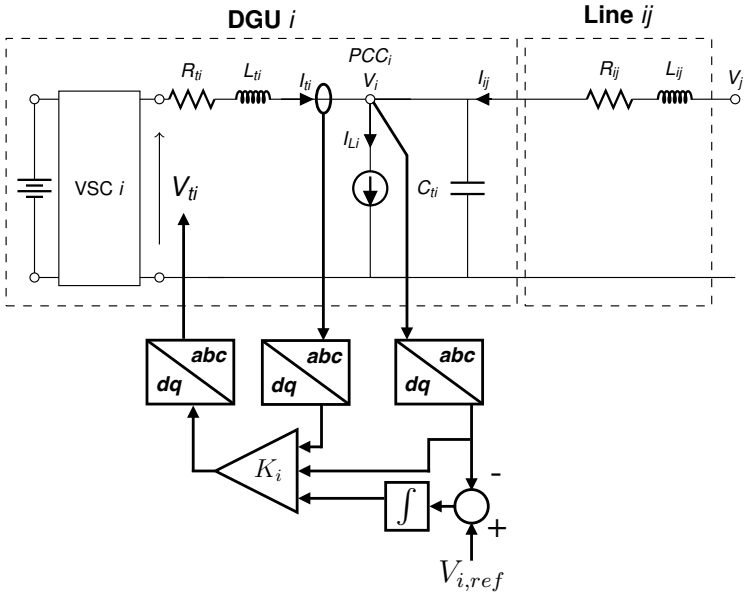

Figure 1: Electrical scheme of DGU i (in the dashed frame) and local PnP voltage and frequency controller.

that the output $y_{[i]} = x_{[i]}$ is measurable, and let term $\xi_{[i]} = \sum_{j\in\mathcal{N}_i} A_{ij}(x_{[j]} - x_{[i]})$ account for the coupling with each DGU $j \in \mathcal{N}_i$. We highlight that the provided model is identical to the one in [1], except that the coupling terms have been embedded in the contribution $\xi_{[i]}$. As regards the matrices in (2), they have the following form

$$A_{ii} = \begin{bmatrix} 0 & \omega_0 & \frac{1}{C_{ti}} & 0 \\ -\omega_0 & 0 & 0 & \frac{1}{C_{ti}} \\ -\frac{1}{L_{ti}} & 0 & -\frac{R_{ti}}{L_{ti}} & \omega_0 \\ 0 & -\frac{1}{L_{ti}} & -\omega_0 & -\frac{R_{ti}}{L_{ti}} \end{bmatrix}, \quad A_{ij} = \frac{1}{C_{ti}} \begin{bmatrix} \frac{R_{ij}}{Z_{ij}^2} & \frac{X_{ij}}{Z_{ij}^2} & \mathbf{0} \\ -\frac{X_{ij}}{Z_{ij}^2} & \frac{R_{ij}}{Z_{ij}^2} & \mathbf{0} \\ \mathbf{0} & \mathbf{0} & \mathbf{0} \end{bmatrix},$$

$$B_i = \begin{bmatrix} \mathbf{0} & \mathbf{0} \\ \frac{1}{L_{ti}} & 0 \\ 0 & \frac{1}{L_{ti}} \end{bmatrix}, \quad M_i = \begin{bmatrix} -\frac{1}{C_{ti}} & 0 \\ 0 & -\frac{1}{C_{ti}} \\ \mathbf{0} & \mathbf{0} \end{bmatrix}, \; C_i = I_4, \; H_i = \begin{bmatrix} 1 & 0 & \mathbf{0} \\ 0 & 1 & \mathbf{0} \end{bmatrix},$$

where $X_{ij} = \omega_0 L_{ij}$ and $Z_{ij} = |R_{ij} + \mathrm{i}X_{ij}|$.
At this point, we can write the ImG model as follows

$$\begin{aligned} \dot{\mathbf{x}}(t) &= \mathbf{A}\mathbf{x}(t) + \mathbf{B}\mathbf{u}(t) + \mathbf{M}\mathbf{d}(t) \\ \mathbf{y}(t) &= \mathbf{C}\mathbf{x}(t) \\ \mathbf{z}(t) &= \mathbf{H}\mathbf{y}(t) \end{aligned} \tag{3}$$

where $\mathbf{x} = (x_{[1]}, \ldots, x_{[N]}) \in \mathbb{R}^{4N}$, $\mathbf{u} = (u_{[1]}, \ldots, u_{[N]}) \in \mathbb{R}^{2N}$, $\mathbf{d} = (d_{[1]}, \ldots, d_{[N]}) \in \mathbb{R}^{2N}$, $\mathbf{y} = (y_{[1]}, \ldots, y_{[N]}) \in \mathbb{R}^{4N}$, $\mathbf{z} = (z_{[1]}, \ldots, z_{[N]}) \in \mathbb{R}^{2N}$. Matrices $\mathbf{A}$, $\mathbf{B}$, $\mathbf{M}$, $\mathbf{C}$ and $\mathbf{H}$ are shown in Appendix A.3 of [23].

3 Design of PnP stabilizing controllers

3.1 Structure of the local regulators

As in [1], in order to track constant references $\mathbf{z_{ref}}(t) = \bar{\mathbf{z}}_{\mathbf{ref}}$, the ImG model is augmented with integrators (see Figure 1, where $z_{ref_{[i]}} = V_{ref,i}$). Hence, we first write the dynamics of the integrators as

$$\begin{aligned}\dot{v}_{[i]}(t) = e_{[i]}(t) &= z_{ref\,[i]}(t) - z_{[i]}(t) \\ &= z_{ref\,[i]}(t) - H_{[i]}C_{[i]}x_{[i]}(t),\end{aligned}$$

and then derive the augmented model of the DGU

$$\hat{\Sigma}^{DGU}_{[i]} : \begin{cases} \dot{\hat{x}}_{[i]}(t) = \hat{A}_{ii}\hat{x}_{[i]}(t) + \hat{B}_i u_{[i]}(t) + \hat{M}_i \hat{d}_{[i]}(t) + \hat{\xi}_{[i]}(t) \\ \hat{y}_{[i]}(t) = \hat{C}_i \hat{x}_{[i]}(t) \\ z_{[i]}(t) = \hat{H}_i \hat{y}_{[i]}(t) \end{cases} \tag{4}$$

where $\hat{x}_{[i]} = [x^T{}_{[i]}, v^T_{[i]}]^T \in \mathbb{R}^6$ is the state, $\hat{y}_{[i]} = \hat{x}_{[i]} \in \mathbb{R}^6$ the measurable output, $\hat{d}_{[i]} = [d^T_{[i]}, z_{ref}{}^T_{[i]}]^T \in \mathbb{R}^4$ the exogenous signals and $\hat{\xi}_{[i]} = \sum_{j\in\mathcal{N}_i} \hat{A}_{ij}(\hat{x}_{[j]} - \hat{x}_{[i]})$. Moreover, matrices in (4) have the form

$$\hat{A}_{ii} = \begin{bmatrix} A_{ii} & \mathbf{0} \\ -H_i C_i & \mathbf{0} \end{bmatrix}, \quad \hat{A}_{ij} = \begin{bmatrix} A_{ij} & \mathbf{0} \\ \mathbf{0} & \mathbf{0} \end{bmatrix}, \quad \hat{B}_i = \begin{bmatrix} B_i \\ \mathbf{0} \end{bmatrix}, \quad \hat{C}_i = \begin{bmatrix} C_i & \mathbf{0} \\ \mathbf{0} & I_2 \end{bmatrix},$$
$$\hat{M}_i = \begin{bmatrix} M_i & \mathbf{0} \\ \mathbf{0} & I_2 \end{bmatrix}, \qquad \hat{H}_i = \begin{bmatrix} H_i & \mathbf{0} \end{bmatrix}.$$

We highlight that, since electrical parameters are positive, the pair $(\hat{A}_{ii}, \hat{B}_i)$ is controllable (see Proposition 2 in [1]). Therefore, system (4) can be stabilized.

As in [1], the overall augmented system is obtained from (4) as

$$\begin{cases} \dot{\hat{\mathbf{x}}}(t) = \hat{\mathbf{A}}\hat{\mathbf{x}}(t) + \hat{\mathbf{B}}\mathbf{u}(t) + \hat{\mathbf{M}}\hat{\mathbf{d}}(t) \\ \hat{\mathbf{y}}(t) = \hat{\mathbf{C}}\hat{\mathbf{x}}(t) \\ \mathbf{z}(t) = \hat{\mathbf{H}}\hat{\mathbf{y}}(t) \end{cases} \tag{5}$$

where $\hat{\mathbf{x}}$, $\hat{\mathbf{y}}$ and $\hat{\mathbf{d}}$ collect variables $\hat{x}_{[i]}$, $\hat{y}_{[i]}$ and $\hat{d}_{[i]}$ respectively, and matrices $\hat{\mathbf{A}}, \hat{\mathbf{B}}, \hat{\mathbf{C}}, \hat{\mathbf{M}}$ and $\hat{\mathbf{H}}$ are derived directly from the systems (4). Finally, we equip each DGU $\hat{\Sigma}^{DGU}_{[i]}$ with the following state-feedback controller

$$\mathcal{C}_{[i]} : \qquad u_{[i]}(t) = K_i \hat{y}_{[i]}(t) = K_i \hat{x}_{[i]}(t)$$

where $K_i = \mathbb{R}^{2\times 6}$.

Note that the computation of $u_{[i]}$ requires the state of $\hat{\Sigma}^{DGU}_{[i]}$ only. Hence, we have that the overall control architecture is decentralized.

3.2 Conditions for ImG stability

If coupling terms $\hat{\xi}_i(t)$ are not present, the asymptotic stability of the overall ImG is guaranteed by simply stabilizing each closed-loop subsystem

$$\dot{\hat{x}}_{[i]}(t) = \underbrace{(\hat{A}_{ii} + \hat{B}_i K_i)}_{F_i} \hat{x}_{[i]}(t) + \hat{M}_i \hat{d}_{[i]}. \tag{6}$$

By direct calculation, one can show that F_i in (6) has the following structure

$$F_i = \left[\begin{array}{c|cc} \mathcal{F}_{11,i} & \mathcal{F}_{12,i} & \mathbf{0}_2 \\ \hline \mathcal{F}_{21,i} & \mathcal{F}_{22,i} & \mathcal{F}_{23,i} \\ -I_2 & \mathbf{0}_2 & \mathbf{0}_2 \end{array}\right] = \left[\begin{array}{c|c} F_{11,i} & F_{12,i} \\ \hline F_{21,i} & F_{22,i} \end{array}\right], \tag{7}$$

with

$$\mathcal{F}_{11,i} = \omega_0 \begin{bmatrix} 0 & 1 \\ -1 & 0 \end{bmatrix} \text{ and } \mathcal{F}_{12,i} = \frac{1}{C_{ti}} I_2. \tag{8}$$

According to Lyapunov theory, system (6) is asymptotically stable if there exists a Lyapunov function $\mathcal{V}_i(\hat{x}_{[i]}) = \hat{x}_{[i]}^T P_i \hat{x}_{[i]}$, with $P_i = P_i^T > 0$ and

$$Q_i = F_i^T P_i + P_i F_i \tag{9}$$

negative definite.

In a real ImG, however, interactions between subsystems exist. In the sequel, we show that asymptotic stability of the overall ImG can be guaranteed by adding the following conditions.

Assumption 1. *Each gain matrix K_i, $i \in \mathcal{D}$ is designed such that matrix P_i in* (9) *has the structure*

$$P_i = \left[\begin{array}{c|c} \eta_i I_2 & \mathbf{0}_2 \\ \hline \mathbf{0}_2 & P_{22,i} \end{array}\right], \tag{10}$$

where the entries of $P_{22,i} \in \mathbb{R}^{4\times 4}$ are arbitrary and $\eta_i > 0$ is a local parameter.

Remark 1. *Assumption 1 amounts to use local separable Lyapunov functions in the form*

$$\mathcal{V}_i(\hat{x}_{[i]}) = \eta_i \hat{x}_{[i],1}^T \hat{x}_{[i],1} + \tilde{x}_{[i]}^T \, P_{22,i} \tilde{x}_{[i]},$$

where $\hat{x}_{[i]} = [\hat{x}_{[i],1}^T, \tilde{x}_{[i]}^T]^T$, $\tilde{x}_{[i]} \in \mathbb{R}^4$.

The second condition regards the values of parameters η_i.

Assumption 2. *Let $\bar{\sigma} > 0$ be a constant parameter, common to all DGUs. Parameters η_i in* (10) *are given by*

$$\eta_i = \bar{\sigma} C_{ti} \qquad \forall i \in \mathcal{D}.$$

The stability analysis continues by showing that, if Assumption 1 holds, Lyapunov theory certifies at most marginal stability of (5). To this purpose, we provide the following Proposition.

Proposition 1. *Under Assumption 1, matrix Q_i in* (9) *cannot be negative definite. Moreover,*

$$Q_i \leq 0 \tag{11}$$

implies that Q_i has the following structure:

$$Q_i = \left[\begin{array}{c|cc} \mathbf{0}_2 & \mathbf{0}_2 & \mathbf{0}_2 \\ \hline \mathbf{0}_2 & \mathcal{Q}_{22,i} & \mathcal{Q}_{23,i} \\ \mathbf{0}_2 & \mathcal{Q}_{23,i} & \mathcal{Q}_{33,i} \end{array}\right] = \left[\begin{array}{c|c} \mathbf{0}_2 & \mathbf{0} \\ \hline \mathbf{0} & Q_{22,i} \end{array}\right]. \tag{12}$$

Proof. By substituting (7) and (10) in (9), it follows that the first two elements on the diagonal of Q_i are zero. Hence Q_i cannot be negative definite. Moreover, from basic linear algebra, if a negative semidefinite matrix has a zero element on its diagonal, the corresponding row and column have zero entries. Then (11) implies (12). □

Next, we consider the overall closed-loop ImG model, given by

$$\begin{cases} \dot{\hat{\mathbf{x}}}(t) = (\hat{\mathbf{A}} + \hat{\mathbf{B}}\mathbf{K})\hat{\mathbf{x}}(t) + \hat{\mathbf{M}}\hat{\mathbf{d}}(t) \\ \hat{\mathbf{y}}(t) = \hat{\mathbf{C}}\hat{\mathbf{x}}(t) \\ \mathbf{z}(t) = \hat{\mathbf{H}}\hat{\mathbf{y}}(t) \end{cases} \tag{13}$$

where $\mathbf{K} = \text{diag}(K_1, \dots, K_N)$. Being $\mathbf{P} = \text{diag}(P_1, \dots, P_N)$, the collective Lyapunov function is

$$\mathcal{V}(\hat{\mathbf{x}}) = \sum_{i=1}^{N} \mathcal{V}_i(\hat{x}_{[i]}) = \hat{\mathbf{x}}^T \mathbf{P} \hat{\mathbf{x}}$$

and, consequently, one has that $\dot{\mathcal{V}}(\hat{\mathbf{x}}) = \hat{\mathbf{x}}^T \mathbf{Q} \hat{\mathbf{x}}$, where

$$\mathbf{Q} = (\hat{\mathbf{A}} + \hat{\mathbf{B}}\mathbf{K})^T \mathbf{P} + \mathbf{P}(\hat{\mathbf{A}} + \hat{\mathbf{B}}\mathbf{K}).$$

From Proposition 1, one has that the matrix $\mathbf{Q}$ cannot be negative definite, and that, at most, it holds

$$\mathbf{Q} \leq 0. \tag{14}$$

However, even if (11) is verified for all $i \in \mathcal{D}$, the inequality (14) might be violated because of the nonzero coupling terms $\hat{A}_{ij}$ in matrix $\hat{\mathbf{A}}$ (see, e.g., the example in Appendix B of [23]). Through the next Proposition, we show that this cannot happen if Assumption 2 is fulfilled.

Proposition 2. *Under Assumptions 1 and 2, if regulators K_i are computed to satisfy* (11) *for all $i \in \mathcal{D}$, then* (14) *holds.*

Proof. We start by decomposing the matrix $\hat{\mathbf{A}}$ as follows

$$\hat{\mathbf{A}} = \hat{\mathbf{A}}_{\mathbf{D}} + \hat{\mathbf{A}}_{\mathbf{\Xi}} + \hat{\mathbf{A}}_{\mathbf{C}}, \tag{15}$$

where (i) $\hat{\mathbf{A}}_{\mathbf{D}} = \text{diag}(\hat{A}_{ii}, \dots, \hat{A}_{NN})$ collects the local dynamics only, (ii) $\hat{\mathbf{A}}_{\mathbf{\Xi}} = \text{diag}(\hat{A}_{\xi 1}, \dots, \hat{A}_{\xi N})$ with

$$\hat{A}_{\xi i} = \frac{1}{C_{ti}} \left[\begin{array}{cc|c} \sum\limits_{j \in \mathcal{N}_i} -\tilde{R}_{ij} & \sum\limits_{j \in \mathcal{N}_i} -\tilde{X}_{ij} & \mathbf{0} \\ \sum\limits_{j \in \mathcal{N}_i} \tilde{X}_{ij} & \sum\limits_{j \in \mathcal{N}_i} -\tilde{R}_{ij} & \mathbf{0} \\ \hline \mathbf{0} & \mathbf{0} & \mathbf{0} \end{array}\right], \tag{16}$$

$\tilde{R}_{ij} = \frac{R_{ij}}{Z_{ij}^2}$ and $\tilde{X}_{ij} = \frac{X_{ij}}{Z_{ij}^2}$, takes into account the dependance of each local state on the neighboring DGUs, and (iii) matrix $\hat{\mathbf{A}}_{\mathbf{C}}$ includes the effect of couplings and is composed by zero blocks on the diagonal and blocks $\hat{A}_{ij}$, $i \neq j$ outside the diagonal.

Our goal is to demonstrate (14), that, using (15), is

$$\underbrace{(\hat{\mathbf{A}}_{\mathbf{D}} + \hat{\mathbf{B}}\mathbf{K})^{\mathbf{T}}\mathbf{P} + \mathbf{P}(\hat{\mathbf{A}}_{\mathbf{D}} + \hat{\mathbf{B}}\mathbf{K})}_{(a)} + \underbrace{\hat{\mathbf{A}}_{\mathbf{\Xi}}^{\mathbf{T}}\mathbf{P} + \mathbf{P}\hat{\mathbf{A}}_{\mathbf{\Xi}}}_{(b)} + \underbrace{\hat{\mathbf{A}}_{\mathbf{C}}^{T}\mathbf{P} + \mathbf{P}\hat{\mathbf{A}}_{\mathbf{C}}}_{(c)} \leq 0. \tag{17}$$

Since (11) holds, we have $(a) = \text{diag}(Q_1, \dots, Q_N) \leq 0$. At this point, we need to study the contribution of matrix $(b) + (c)$ in (17). By construction (recalling (10) and (16)), matrix (b) is block diagonal, collecting on its diagonal blocks in the form

$$\begin{aligned} \hat{A}_{\xi i}^T P_i + P_i \hat{A}_{\xi i} &= \left[\begin{array}{cc|c} -\frac{\eta_i}{C_{ti}} \sum\limits_{j \in \mathcal{N}_i} \left(\tilde{R}_{ij} + \tilde{R}_{ij}\right) & \frac{\eta_i}{C_{ti}} \sum\limits_{j \in \mathcal{N}_i} \left(\tilde{X}_{ij} - \tilde{X}_{ij}\right) & \mathbf{0} \\ \frac{\eta_i}{C_{ti}} \sum\limits_{j \in \mathcal{N}_i} \left(\tilde{X}_{ij} - \tilde{X}_{ij}\right) & -\frac{\eta_i}{C_{ti}} \sum\limits_{j \in \mathcal{N}_i} \left(\tilde{R}_{ij} + \tilde{R}_{ij}\right) & \mathbf{0} \\ \hline \mathbf{0} & \mathbf{0} & \mathbf{0} \end{array}\right] \\ &= \left[\begin{array}{cc|c} -\sum\limits_{j \in \mathcal{N}_i} 2\tilde{\eta}_{ij} & 0 & \mathbf{0} \\ 0 & -\sum\limits_{j \in \mathcal{N}_i} 2\tilde{\eta}_{ij} & \mathbf{0} \\ \hline \mathbf{0} & \mathbf{0} & \mathbf{0} \end{array}\right], \end{aligned} \tag{18}$$

with $\tilde{\eta}_{ij} = \frac{\eta_i}{C_{ti}}\tilde{R}_{ij} = \bar{\sigma}\tilde{R}_{ij}$. Regarding matrix (c), we have that each the block in position (i,j) is equal to

$$\begin{cases} P_i\hat{A}_{ij} + \hat{A}_{ji}^T P_j & \text{if } j \in \mathcal{N}_i \\ \mathbf{0} & \text{otherwise} \end{cases} \tag{19}$$

In particular, recalling Assumption 2, by direct calculation, it results

$$\begin{aligned} P_i\hat{A}_{ij} + \hat{A}_{ji}^T P_j &= \left[\begin{array}{cc|c} \frac{\eta_i}{C_{ti}}\tilde{R}_{ij} + \frac{\eta_j}{C_{tj}}\tilde{R}_{ji} & 0 & \mathbf{0} \\ 0 & \frac{\eta_i}{C_{ti}}\tilde{R}_{ij} + \frac{\eta_j}{C_{tj}}\tilde{R}_{ji} & \mathbf{0} \\ \hline \mathbf{0} & \mathbf{0} & \mathbf{0} \end{array}\right] = \\ &= \left[\begin{array}{cc|c} \tilde{\eta}_{ij} + \tilde{\eta}_{ji} & 0 & \mathbf{0} \\ 0 & \tilde{\eta}_{ij} + \tilde{\eta}_{ji} & \mathbf{0} \\ \hline \mathbf{0} & \mathbf{0} & \mathbf{0} \end{array}\right] = \left[\begin{array}{cc|c} 2\tilde{\eta}_{ij} & 0 & \mathbf{0} \\ 0 & 2\tilde{\eta}_{ij} & \mathbf{0} \\ \hline \mathbf{0} & \mathbf{0} & \mathbf{0} \end{array}\right]. \end{aligned} \tag{20}$$

By looking at (18) and (20), we observe that only the elements in position $(1,1)$ and $(2,2)$ of each 6×6 block of $(b)+(c)$ can be different from zero. Therefore, the positive/negative definiteness of the $6N \times 6N$ matrix $(b)+(c)$ can be equivalently studied by considering the $2N \times 2N$ matrix

$$\mathcal{L} = \begin{bmatrix} \Phi_{11} & \Phi_{12} & \dots & \Phi_{1N} \\ \Phi_{21} & \ddots & \ddots & \vdots \\ \vdots & \ddots & \Phi_{N-1\ N-1} & \Phi_{N-1\ N} \\ \Phi_{N1} & \dots & \Phi_{N\ N-1} & \Phi_{NN} \end{bmatrix}, \tag{21}$$

obtained by deleting the last four rows and columns in each block of $(b)+(c)$. In particular, we can write (21) as $\mathcal{L} = \mathcal{M} + \mathcal{G}$, with $\mathcal{M} = \text{diag}(\Phi_{11}, \dots, \Phi_{NN})$,

$$\Phi_{ii} = \begin{bmatrix} \sum_{j \in \mathcal{N}_i} -2\tilde{\eta}_{ij} & 0 \\ 0 & \sum_{j \in \mathcal{N}_i} -2\tilde{\eta}_{ij} \end{bmatrix}$$

and

$$\mathcal{G} = \begin{bmatrix} \mathbf{0} & \Phi_{12} & \dots & \Phi_{1N} \\ \Phi_{21} & \mathbf{0} & \ddots & \vdots \\ \vdots & \ddots & \ddots & \Phi_{N-1\ N} \\ \Phi_{N1} & \dots & \Phi_{N\ N-1} & \mathbf{0} \end{bmatrix}.$$

We highlight that, from (19) and (20), blocks Φ_{ij}, $i \neq j$, are equal to

$$\Phi_{ij} = \begin{cases} \begin{bmatrix} 2\tilde{\eta}_{ij} & 0 \\ 0 & 2\tilde{\eta}_{ij} \end{bmatrix} & \text{if } j \in \mathcal{N}_i \\ \mathbf{0}_2 & \text{otherwise} \end{cases}$$

Next, we notice that $\mathcal{L}$ is symmetric, with non negative off-diagonal elements and zero row and column sum. In other words, $\mathcal{L}$ is a Laplacian matrix [24], and, as such, it is negative semidefinite. This allows us to show that (17) (and, equivalently, (14)) holds. □

Remark 2. *The proof of Proposition 2 reveals that, under Assumptions 1 and 2, interactions between local Lyapunov functions $\mathcal{V}_i(\hat{x}_{[i]})$ due to terms $\hat{A}_{ij}$, $i \neq j$, take the form of a weighted Laplacian matrix associated to the graph $\mathcal{G}_{el}$. Furthermore, differently from the idea in [1] of nullifying interactions by choosing $\eta_i > 0$ in* (10) *sufficiently small, here* (14) *holds true even if parameters η_i are large.*

In order to show the asymptotic stability of the ImG, we need to complement Proposition 2 with the applications of the LaSalle invariance theorem. This will be done in Theorem 1, that will rely on the next two Propositions characterizing states $\hat{\mathbf{x}}$ yielding $\dot{\mathcal{V}}(\hat{\mathbf{x}}) = 0$.

Proposition 3. *Let $f_i(v_i) = v_i^T Q_{22,i} v_i$, with $v_i \in \mathbb{R}^4$, and let Assumptions 1 and 2 hold. If* (11) *is guaranteed and $Q_{22,i}\big|_{\mathrm{Im}(F_{22,i}^T)}$ is invertible, then*

$$f_i(\bar{v}_i) = 0 \Longleftrightarrow \bar{v}_i \in \mathrm{Ker}(F_{22,i}).$$

Proof. For the sake of simplicity, in the sequel we omit the subscript i.
Step 1: We start by proving that

$$\bar{v} \in \mathrm{Ker}(F_{22}) \Longrightarrow f(\bar{v}) = 0. \tag{22}$$

To do so, we first replace (7) and (10) in (9), thus obtaining

$$Q_{22} = F_{22}^T P_{22} + P_{22} F_{22}.$$

Then, we write

$$\begin{aligned} f(\bar{v}) &= \bar{v}^T Q_{22} \bar{v} = \\ &= \bar{v}^T F_{22}^T P_{22} \bar{v} + \bar{v}^T P_{22} F_{22} \bar{v} = 2\bar{v}^T P_{22} \underbrace{F_{22}\bar{v}}_{=0} = 0. \end{aligned}$$

Step 2: Next, we show that

$$f(\bar{v}) = 0 \Longrightarrow \bar{v} \in \mathrm{Ker}(F_{22}). \tag{23}$$

To this aim, we reformulate the condition $f(\bar{v}) = 0$ in (23). In particular, from basic linear algebra, we have the following orthogonal decomposition induced by F_{22}

$$\mathbb{R}^4 = \mathrm{Im}(F_{22}^T) \oplus \mathrm{Ker}(F_{22}),$$

which allows us to write any vector $v \in \mathbb{R}^4$ as

$$v = \hat{v} + \tilde{v}, \quad \hat{v} \in \mathrm{Im}(F_{22}^T), \tilde{v} \in \mathrm{Ker}(F_{22}). \tag{24}$$

Now, since we are assuming that Q is negative semidefinite and structured as in (12), vectors $\bar{v}$ satisfying $f(\bar{v}) = 0$ also maximize $f(\cdot)$. Hence,

$$f(\bar{v}) = 0 \Longleftrightarrow \frac{\mathrm{d}f}{\mathrm{d}t}(\bar{v}) = Q_{22}\bar{v} = \mathbf{0}, \tag{25}$$

which, decomposing $\bar{v}$ as in (24), translates into

$$f(\bar{v}) = 0 \Longleftrightarrow Q_{22}\hat{v} + \underbrace{Q_{22}\tilde{v}}_{=\mathbf{0}} = \mathbf{0}. \tag{26}$$

Notice that $Q_{22}\tilde{v} = \mathbf{0}$ in (26) comes from the fact that $\tilde{v} \in \mathrm{Ker}(F_{22})$. In particular, from (22), we know that $f(\tilde{v}) = 0$, and hence condition (25) must hold for $\bar{v} = \tilde{v}$.

At this point, using (26), we can rewrite (23) as follows

$$Q_{22}\hat{v} = \mathbf{0} \Longrightarrow \bar{v} \in \mathrm{Ker}(F_{22}),$$

which, since $\bar{v} \in \mathrm{Ker}(F_{22}) \Longleftrightarrow \hat{v} = \mathbf{0}$, finally becomes

$$Q_{22}\hat{v} = \mathbf{0} \Longrightarrow \hat{v} = \mathbf{0}. \tag{27}$$

Since $Q_{22,i}\big|_{\mathrm{Im}(F_{22,i}^T)}$ is invertible, (27) is verified. The proof ends by observing that (27) is equivalent to (23). □

Proposition 4. *Let $g_i(w_i) = w_i^T Q_i w_i$, with $w_i \in \mathbb{R}^6$, and let the same assumptions of Proposition 3 hold. Then, only vectors $\bar{w}_i$ in the form*

$$\bar{w}_i = \begin{bmatrix} \alpha_i^T & \beta_i^T & \gamma_i^T \end{bmatrix}^T$$

with $\alpha_i, \beta_i, \gamma_i \in \mathbb{R}^2$ and $\mathcal{F}_{22,i}\beta_i + \mathcal{F}_{23,i}\gamma_i = \mathbf{0}$, fulfill

$$g_i(\bar{w}_i) = 0. \tag{28}$$

Proof. As for the proof of Proposition 3, we omit the subscript i. Using (12), we write

$$g(w) = \left[\begin{array}{c|c} w_1^T & w_2^T \end{array}\right] \left[\begin{array}{c|c} \mathbf{0}_2 & \mathbf{0} \\ \hline \mathbf{0} & Q_{22} \end{array}\right] \left[\begin{array}{c} w_1 \\ \hline w_2 \end{array}\right], \tag{29}$$

where $w_2 \in \mathbb{R}^4$. Since Q is negative semidefinite, vectors $\bar{w}$ satisfying (28) also maximize $g(\cdot)$. Hence, it must hold $\frac{\mathrm{d}g}{\mathrm{d}w}(\bar{w}) = Q\bar{w} = \mathbf{0}$, i.e.

$$\left[\begin{array}{c|c} \mathbf{0}_2 & \mathbf{0} \\ \hline \mathbf{0} & Q_{22} \end{array}\right] \left[\begin{array}{c} \bar{w}_1 \\ \hline \bar{w}_2 \end{array}\right] = 0. \tag{30}$$

Obviously, a set of solutions to (28) and (30) is composed of vectors

$$\bar{w} = \begin{bmatrix} \alpha^T & \mathbf{0} \end{bmatrix}^T, \quad \alpha \in \mathbb{R}^2. \tag{31}$$

Moreover, from (29), we have that (28) is also verified if there exist vectors

$$\tilde{w} = \left[\begin{array}{c|c} w_1^T & \underline{w}_2^T \end{array}\right]^T, \quad \underline{w}_2 \in \mathbb{R}^4, \underline{w}_2 \neq \mathbf{0}, \tag{32}$$

such that

$$\underline{w}_2^T Q_{22} \underline{w}_2 = 0, \tag{33}$$

$\forall w_1 \in \mathbb{R}^2$. At this point, we exploit the result of Proposition 3. We know, in fact, that vectors $\underline{w}_2$ satisfying (33) belong to $\mathrm{Ker}(F_{22})$, which can be characterized as follows

$$\begin{aligned} \mathrm{Ker}(F_{22}) &= \{x \in \mathbb{R}^4 : \begin{bmatrix} \mathcal{F}_{22} & \mathcal{F}_{23} \\ \mathbf{0}_2 & \mathbf{0}_2 \end{bmatrix} x = \mathbf{0}\} = \\ &= \{x \in \mathbb{R}^4 : x = \begin{bmatrix} \beta^T & \gamma^T \end{bmatrix}^T, \beta, \gamma \in \mathbb{R}^2, \mathcal{F}_{22}\beta + \mathcal{F}_{23}\gamma = \mathbf{0}\}. \end{aligned} \tag{34}$$

The proof concludes by merging (31) and (32) (with $\underline{w}_2$ as in (34)). □

Theorem 1. *If Assumptions 1 and 2 are fulfilled, the graph $\mathcal{G}_{el}$ is connected,* (11) *holds, $Q_{22,i}\big|_{\mathrm{Im}(F_{22,i}^T)}$ is invertible and $\det(\mathcal{F}_{22,i}\mathcal{F}_{21,i} - \mathcal{F}_{23,i}) \neq 0$, $\forall i \in \mathcal{D}$, the origin of* (13) *is asymptotically stable.*

Proof. By means of Proposition 2, we have shown that (14) holds. Therefore, we aim to use the LaSalle invariance Theorem [25] to show that the origin of the ImG is attractive.

Let us compute the set $R = \{\mathbf{x} \in \mathbb{R}^{6N} : \mathbf{x}^T \mathbf{Q} \mathbf{x} = 0\}$, which, using (17), can be written as

$$\begin{aligned} R &= \{\mathbf{x} : \mathbf{x}^T \left((a) + (b) + (c)\right) \mathbf{x} = 0\} \\ &= \{\mathbf{x} : \mathbf{x}^T (a) \mathbf{x} + \mathbf{x}^T (b) \mathbf{x} + \mathbf{x}^T (c) \mathbf{x} = 0\} \\ &= \underbrace{\{\mathbf{x} : \mathbf{x}^T (a) \mathbf{x} = 0\}}_{X_1} \cap \underbrace{\{\mathbf{x} : \mathbf{x}^T \left[(b) + (c)\right] \mathbf{x} = 0\}}_{X_2}, \end{aligned} \tag{35}$$

and first focus on characterizing the vectors of set X_1. Recalling that $(a) = \text{diag}(Q_1, \dots, Q_N)$, we can exploit Proposition 4, thus having

$$X_1 = \{\mathbf{x} : \mathbf{x} = \left[\begin{array}{ccc|c|ccc} \alpha_1^T & \beta_1^T & \gamma_1^T & \cdots & \alpha_N^T & \beta_N^T & \gamma_N^T \end{array} \right]^T, \alpha_i, \beta_i, \gamma_i \in \mathbb{R}^2, \mathcal{F}_{22,i}\beta_i + \mathcal{F}_{23,i}\gamma_i = 0\}.$$

Next, we focus on the elements of X_2. We have seen that the term $(b) + (c)$ is an "expansion" of the Laplacian matrix in (21), obtained by augmenting each 2×2 block Φ_{ij} of $\mathcal{L}$ with zero rows and columns, so as to retrieve blocks of dimension 6×6. It follows that, by construction, X_2 contains vectors in the form

$$\tilde{\mathbf{x}} = \left[\begin{array}{ccc|c|ccc} \mathbf{0} & \tilde{x}_{12}^T & \tilde{x}_{13}^T & \cdots & \mathbf{0} & \tilde{x}_{N2}^T & \tilde{x}_{N3}^T \end{array} \right]^T, \quad \tilde{x}_{i2}, \tilde{x}_{i3} \in \mathbb{R}^2, \forall i \in \mathcal{D}. \tag{36}$$

Moreover, since the kernel of the Laplacian matrix of a connected graph contains only vectors with identical entries [24], we also have that

$$\{\bar{\mathbf{x}} = \left[\begin{array}{cc|c|cc} \bar{x}^T & \mathbf{0}\ \mathbf{0} & \cdots & \bar{x}^T & \mathbf{0}\ \mathbf{0} \end{array} \right]^T, \ \bar{x} \in \mathbb{R}^2\} \subset X_2. \tag{37}$$

Next, by merging (36) and (37), we obtain

$$X_2 = \{\mathbf{x} : \mathbf{x} = \left[\begin{array}{ccc|c|ccc} \bar{x}^T & \tilde{x}_{12}^T & \tilde{x}_{13}^T & \cdots & \bar{x}^T & \tilde{x}_{N2}^T & \tilde{x}_{N3}^T \end{array} \right]^T, \bar{x}, \tilde{x}_{i2}, \tilde{x}_{i3} \in \mathbb{R}^2\},$$

and then, from (35), it follows

$$R = \{\mathbf{x} : \mathbf{x} = \left[\begin{array}{ccc|c|ccc} \bar{\alpha}^T & \beta_1^T & \gamma_1^T & \cdots & \bar{\alpha}^T & \beta_N^T & \gamma_N^T \end{array} \right]^T, \bar{\alpha}, \beta_i, \gamma_i \in \mathbb{R}^2, \mathcal{F}_{22,i}\beta_i + \mathcal{F}_{23,i}\gamma_i = \mathbf{0}\}. \tag{38}$$

For concluding the proof, we must show that the largest invariant set $M \subseteq R$ is the origin. To this purpose, we consider (6), include coupling terms $\hat{\xi}_{[i]}$ and neglect inputs. Then, we choose the initial state $\hat{\mathbf{x}}(0) = \left[\hat{x}_1^T(0) | \dots | \hat{x}_N^T(0)\right]^T \in R$, where, according to (38), $\hat{x}_i(0) = \left[\begin{array}{ccc} \bar{\alpha}^T & \beta_i^T & \gamma_i^T \end{array} \right]^T$, $i = 1, \dots, N$. Our aim is to find conditions on the elements of $\hat{\mathbf{x}}(0)$ that must hold in order to guarantee $\dot{\hat{\mathbf{x}}} \in R$. Recalling (6) and (7), we compute

$$\begin{aligned} \dot{\hat{x}}_i(0) &= F_i \hat{x}_i(0) + \sum_{j \in \mathcal{N}_i} \underbrace{\hat{A}_{ij} \left(\hat{x}_j(0) - \hat{x}_i(0)\right)}_{=0} = \\ &= \begin{bmatrix} \mathcal{F}_{11,i} & \mathcal{F}_{12,i} & \mathbf{0} \\ \mathcal{F}_{21,i} & \mathcal{F}_{22,i} & \mathcal{F}_{23,i} \\ -I_2 & \mathbf{0} & \mathbf{0} \end{bmatrix} \begin{bmatrix} \bar{\alpha} \\ \beta_i \\ \gamma_i \end{bmatrix} = \begin{bmatrix} \mathcal{F}_{11,i}\bar{\alpha} + \mathcal{F}_{12,i}\beta_i \\ \mathcal{F}_{21,i}\bar{\alpha} + \underbrace{\mathcal{F}_{22,i}\beta_i + \mathcal{F}_{23,i}\gamma_i}_{=\mathbf{0}} \\ -\bar{\alpha} \end{bmatrix}. \end{aligned} \tag{39}$$

In order to have $\dot{\hat{x}}_i(0) \in R$, it must hold, $\forall i, j \in \mathcal{D}$

$$\mathcal{F}_{11,i}\bar{\alpha} + \mathcal{F}_{12,i}\beta_i = \mathcal{F}_{11,j}\bar{\alpha} + \mathcal{F}_{12,j}\beta_j$$

which, from (8), implies

$$\frac{1}{C_{ti}}\beta_i = \frac{1}{C_{tj}}\beta_j.$$

This means that there is $\bar{\beta} \in \mathbb{R}^2$, such that $C_{ti}\bar{\beta} = \beta_i$, $\forall i \in \mathcal{D}$. Moreover, $\dot{\hat{x}}_i(0) \in R$ implies the following relation between the two last subvectors in (39)

$$\mathcal{F}_{22,1}(\mathcal{F}_{21,i}\bar{\alpha}) + \mathcal{F}_{23,i}(-\bar{\alpha}) = \mathbf{0}.$$

Using the assumption that $(\mathcal{F}_{22,1}\mathcal{F}_{21,i} - \mathcal{F}_{23,i})$ is invertible, one has $\bar{\alpha} = \mathbf{0}$. Therefore, in order to have $\dot{\hat{x}}_i(0) \in R$, it must hold $\hat{x}_i(0) = \left[\begin{array}{ccc} \mathbf{0} & \bar{\beta}^T & \gamma_i^T \end{array} \right]^T$, with $\mathcal{F}_{22,i}C_{ti}\bar{\beta} + \mathcal{F}_{23,i}\gamma_i = \mathbf{0}$. Let

$$S = \{\mathbf{x} : \mathbf{x} = \left[\ \mathbf{0}\ C_{t1}\bar{\beta}^T\ \gamma_1^T\ \mid\ \cdots\ \mid\ \mathbf{0}\ C_{tN}\bar{\beta}^T\ \gamma_1^T\ \right]^T, \mathcal{F}_{22,i}C_{ti}\bar{\beta} + \mathcal{F}_{23,i}\gamma_i = \mathbf{0}\}. \tag{40}$$

Since $M \subseteq S$, we pick $\tilde{\mathbf{x}}(0) \in S$ and impose $\dot{\tilde{\mathbf{x}}}(0) \in S$. This gives

$$\dot{\tilde{x}}_i(0) = F_i \begin{bmatrix} \mathbf{0} \\ C_{ti}\bar{\beta} \\ \gamma_i \end{bmatrix} = \begin{bmatrix} \bar{\beta} \\ \mathbf{0} \\ \mathbf{0} \end{bmatrix}, \forall i \in \mathcal{D}.$$

It follows that $\dot{\tilde{\mathbf{x}}}(0) \in S$ only if $\bar{\beta} = \mathbf{0}$. Since $M \subseteq S$, from (40), one has $M = \{0\}$. □

3.3 Computation of local controllers through numerical optimization

The problem of computing matrices K_i and P_i so as to fulfill the assumptions of Theorem 1, can be split into two subproblems.

SP1: Let parameters η_i be computed as in Assumption 2, where the ImG parameter $\bar{\sigma}$ is assumed to be fixed. Compute matrices K_i and P_i so that Assumption 1 and inequality (11) hold.

SP2: Check if $Q_{22,i}\big|_{\mathrm{Im}(F_{22,i}^T)}$ and $(\mathcal{F}_{22,i}\mathcal{F}_{21,i} - \mathcal{F}_{23,i})$ are invertible maps.

SP1 can be recast into an LMI problem. To this purpose, we enforce, when possible, a margin of robustness by designing controllers K_i such that inequality

$$(\hat{A}_{ii} + \hat{B}_i K_i)^T P_i + P_i(\hat{A}_{ii} + \hat{B}_i K_i) + \Gamma_i^{-1} \leq 0,$$

with $\Gamma_i = \mathrm{diag}(\gamma_{1i}, \gamma_{2i}, \gamma_{3i}, \gamma_{4i}, \gamma_{5i}, \gamma_{6i})$, is verified for $\gamma_{ki} \geq 0$, $k = 1, \ldots, 6$ and matrix P_i structured as in (10). Then, we solve the following LMI problem

$$\mathcal{O}_i : \min_{Y_i, G_i, \{\gamma_{ki}\}_{k=1}^6, \beta_i, \zeta_i} \quad \sum_{k=1}^{6} \alpha_{ki}\gamma_{ki} + \alpha_{7i}\beta_i + \alpha_{8i}\zeta_i$$

$$Y_i = \begin{bmatrix} \eta_i^{-1} & 0 & 0 & 0 & 0 & 0 \\ 0 & \eta_i^{-1} & 0 & 0 & 0 & 0 \\ 0 & 0 & \bullet & \bullet & \bullet & \bullet \\ 0 & 0 & \bullet & \bullet & \bullet & \bullet \\ 0 & 0 & \bullet & \bullet & \bullet & \bullet \\ 0 & 0 & \bullet & \bullet & \bullet & \bullet \end{bmatrix} > 0 \tag{41a}$$

$$\begin{bmatrix} Y_i\hat{A}_{ii}^T + G_i^T\hat{B}_i^T + \hat{A}_{ii}Y_i + \hat{B}_i G_i & Y_i \\ Y_i & -\Gamma_i \end{bmatrix} \leq 0 \tag{41b}$$

$$\begin{bmatrix} -\beta_i I & G_i^T \\ G_i & -I \end{bmatrix} < 0, \quad \begin{bmatrix} Y_i & I \\ I & \zeta_i I \end{bmatrix} > 0 \tag{41c}$$

$$\gamma_{ki} \geq 0, i = 1, \ldots, 6, \quad \beta_i > 0, \quad \zeta_i > 0 \tag{41d}$$

where α_{ji}, $j = 1 \ldots, 8$ represent positive weights and $\bullet$ are arbitrary entries. As shown in [1], feasible solutions of (41) provide $P_i = Y_i^{-1}$, with the structure (10) and $K_i = Y_i^{-1}G_i$. Furthermore, the cost penalizes aggressive control actions because it minimizes β_i and ζ_i that, in view of (41c), provide the bound $||K_i||_2 \leq \sqrt{\beta_i}\zeta_i$ [1]. Problem SP2 provides constraints that can be either verified a posteriori or added to (41). While the latter solution is preferable, constraints are nonlinear in the optimization variables of problem $\mathcal{O}_i$, and therefore spoil the LMI nature of (41). Future research will focus on finding convex formulations (or convex approximations) of conditions in SP2.

We highlight that the computation of controller $\mathcal{C}_{[i]}$ is completely decentralized (i.e. independent from the synthesis of controllers $\mathcal{C}_{[j]}$, $j \neq i$.), as constraints in (41) depend upon local fixed matrices ($\hat{A}_{ii}$, $\hat{B}_i$) and local design parameters (α_{ki}, $k = 1, \ldots, 8$.).

Finally, if problems SP1 and SP2 are feasible for all DGUs, then the overall closed-loop QSL-ImG is asymptotically stable.

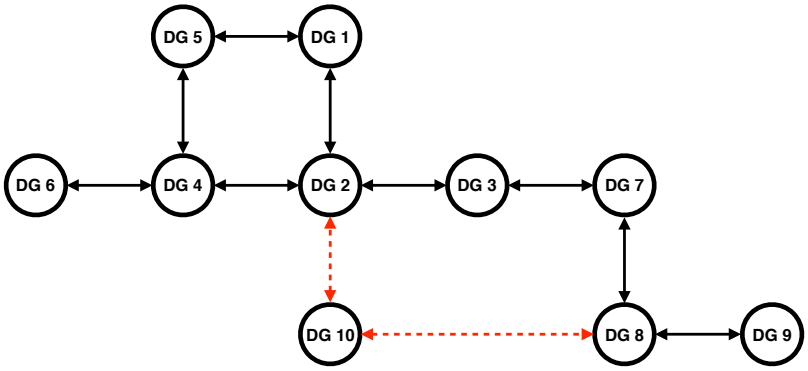

Figure 2: Scheme of the ImG composed of DGUs 1-9 until $t = 7.5$ s (in black), and of 10 DGUs after the plugging-in of $\hat{\Sigma}^{DGU}_{[10]}$ (in red).

Controllers $\mathcal{C}_{[i]}$ yield a closed-loop DGU model that is linear. Hence, it can be easily complemented with pre-filters (for tuning the local bandwidth) and load-current compensators. These enhancements (not used in the simulation in Section 4) are described in [23].

3.4 PnP operations

In this Section, we describe the operations that are required for adding and removing DGUs, while preserving the stability of the mG.

Plugging-in operation Suppose that we want to connect a new DGU (say $\hat{\Sigma}^{DGU}_{[N+1]}$) to the ImG and let $\mathcal{N}_{[N+1]}$ be the set of DGUs that will be directly connected to $\hat{\Sigma}^{DGU}_{[N+1]}$ through power lines. Then, we first solve subproblems SP1 and SP2 in Section 3.3 for the new unit. If one is infeasible, the plug-in is denied. Otherwise, differently from the procedure in [1], DGUs in $\mathcal{N}_{[N+1]}$ do not have to retune their local controllers in order to fulfill stability conditions.

Unplugging operation When a DGU is disconnected, this has no impact on the controllers of the remaining units, if they are designed using the line-independent method described in Section 3.3. Therefore, in view of Theorem 1, stability of the ImG is preserved as far as the graph $\mathcal{G}_{el}$ is still connected after the unplugging of the DGU.

4 Simulation results

In this Section, we study the performance of the proposed PnP controllers. We consider the ImG in Figure 2, composed of 10 DGUs. All DGUs feed RL loads, except DGU 2 which is connected to a three-phase six-pulse diode rectifier. We notice a loop in the network that complicates the voltage regulation. Furthermore, DGUs are non-identical and all the electrical parameters are similar to those of the 11-DGUs example in [1]. The simulation (conducted in PSCAD) starts with DGUs 1-9 connected together and equipped with PnP controllers $\mathcal{C}_{[i]}$, $i = 1, \ldots, 9$.

As a first test, we validate the capability of PnP regulators to deal with real-time plugging-in of DGUs. Therefore, at time $t = 7.5$ s, we simulate the connection of DGU 10, with DGUs 2 and 8 (see Figure 2). Before this event, as described in Section 3.4, we solve subproblems SP1 and SP2 for computing $\mathcal{C}_{[10]}$ and, since both of them result to be feasible, the connection of DGU 10 is allowed. The dq component of the voltages at PCCs 2, 8, 10 are shown in Figures 3a, 3b and 3c, respectively. Notably, we notice very small deviations of the DGUs voltages from their respective reference signals ($V^d_{2,ref} = 0.9$ pu, $V^q_{2,ref} = 0.5$ pu, $V^q_{8,ref} = 0.7$ pu, $V^q_{8,ref} = 0.6$ pu, and $V^q_{10,ref} = 0.8$ pu, $V^q_{10,ref} = 0.6$ pu). Furthermore, these deviations are compensated after a short transient.

Next, in order to assess the robustness of the PnP-controlled ImG to load dynamics, at time $t = 10$ s we simulate an abrupt switch of the RL load at PCC 10 (i.e. from $R = 60\ \Omega$, $L = 0.02$ mH to $R = 120\ \Omega$, $L = 0.02$ mH). From Figures 3a, 3b and 3c, we notice that the d and q components of the voltages at PCCs 2, 8 and 10, do not significantly deviate from their references, thus revealing us that step changes in the loads can be rapidly absorbed. Figure 3d shows that the real-time plugging-in of DGU 10 and the load change at its PCC produce minor effects also on the frequency profiles of the PCC voltages. Notably, we notice that PnP regulators are capable to promptly restore the frequencies to the reference value (50 Hz), guaranteeing, overall, variations smaller than 0.2 Hz. In a similar way, we do not notice significant deviations from the reference RMS voltages (see Figure 3e). Finally, Figure 3f provides a plot of the Total Harmonic Distortion (THD) of the voltage at PCC 2, whose local load is nonlinear. We notice that the THD always remains below 5%, which is the maximum limit recommended by IEEE standards [26].

5 Conclusions

In this paper, we presented a decentralized control approach to voltage and frequency stabilization in AC ImG. Differently from the PnP methodology in [1], the presented procedure guarantees overall ImG stability while computing local controllers in a line-independent fashion. Future research will focus on studying how to couple PnP local regulators with a higher control layer for power flow regulation among DGUs.

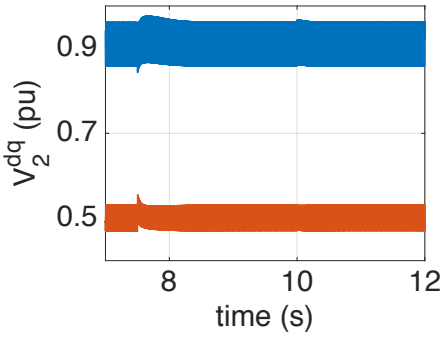

(a) d and q components of the voltage at PCC_2.

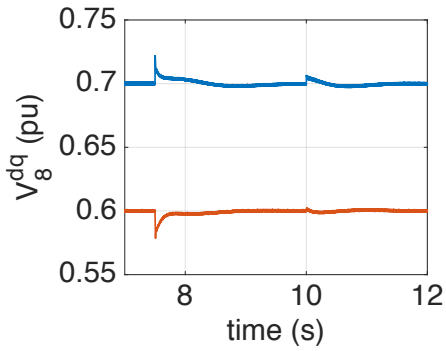

(b) d and q components of the voltage at PCC_8.

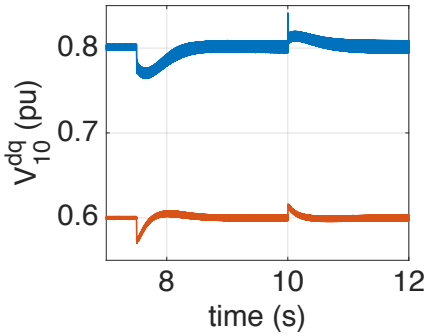

(c) d and q components of the voltage at PCC_{10}.

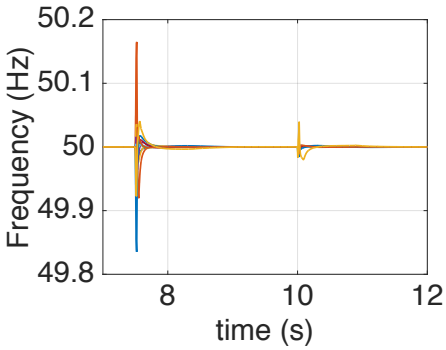

(d) Frequency of phase a at the PCCs.

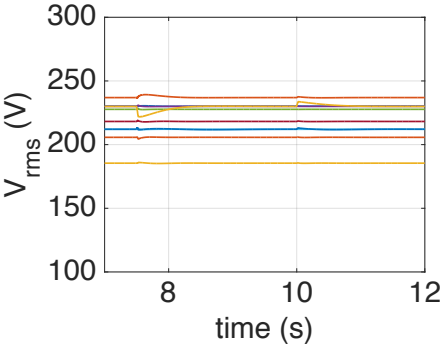

(e) RMS voltages of phase a at the PCCs.

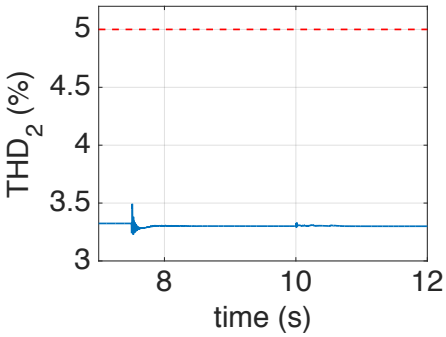

(f) THD of phase a of the voltage at PCC_2.

Figure 3: Performance of PnP voltage and frequency control.

References

[1] S. Riverso, F. Sarzo, and G. Ferrari-Trecate, "Plug-and-play voltage and frequency control of islanded microgrids with meshed topology," *IEEE Transactions on Smart Grid*, vol. 6, no. 3, pp. 1176–1184, May 2015.

[2] J. M. Guerrero, M. Chandorkar, T. Lee, and P. C. Loh, "Advanced Control Architectures for Intelligent Microgrids — Part I: Decentralized and Hierarchical Control," *IEEE Transactions on Industrial Electronics*, vol. 60, no. 4, pp. 1254–1262, 2013.

[3] J. Schiffer, R. Ortega, A. Astolfi, J. Raisch, and T. Sezi, "Conditions for stability of droop-controlled inverter-based microgrids," *Automatica*, vol. 50, no. 10, pp. 2457–2469, 2014.

[4] J. W. Simpson-Porco, F. Dörfler, and F. Bullo, "Synchronization and power sharing for droop-controlled inverters in islanded microgrids," *Automatica*, vol. 49, no. 9, pp. 2603–2611, 2013.

[5] M. Andreasson, R. Wiget, D. V. Dimarogonas, K. H. Johansson, and G. Andersson, "Distributed primary frequency control through multi-terminal hvdc transmission systems," in *2015 American Control Conference (ACC)*, July 2015, pp. 5029–5034.

[6] A. H. Etemadi, E. J. Davison, and R. Iravani, "A Decentralized Robust Control Strategy for Multi-DER Microgrids - Part I: Fundamental Concepts," *IEEE Transactions on Power Delivery*, vol. 27, no. 4, pp. 1843–1853, 2012.

[7] M. Babazadeh and H. Karimi, "A Robust Two-Degree-of-Freedom Control Strategy for an Islanded Microgrid," *IEEE Transactions on Power Delivery*, vol. 28, no. 3, pp. 1339–1347, 2013.

[8] V. Nasirian, Q. Shafiee, J. M. Guerrero, F. L. Lewis, and A. Davoudi, "Droop-free distributed control for ac microgrids," *IEEE Transactions on Power Electronics*, vol. 31, no. 2, pp. 1600–1617, Feb 2016.

[9] IEEE1588, "IEEE draft standard profile for use of IEEE 1588 precision time protocol in power system applications," *IEEE PC37.238/D21.1, August 2016*, pp. 1–42, Jan 2016.

[10] J. Kumagai, "The rise of the personal power plant," *IEEE Spectrum, The smarter grid*, vol. 51, no. 6, pp. 54–49, 2014.

[11] M. S. Sadabadi, Q. Shafiee, and A. Karimi, "Plug-and-play voltage stabilization in inverter-interfaced microgrids via a robust control strategy," *IEEE Transactions on Control Systems Technology*, vol. PP, no. 99, pp. 1–11, 2016.

[12] M. Tucci, S. Riverso, J. C. Vasquez, J. M. Guerrero, and G. Ferrari-Trecate, "A decentralized scalable approach to voltage control of DC islanded microgrids," *IEEE Transactions on Control Systems Technology*, vol. 24, no. 6, pp. 1965–1979, Nov 2016.

[13] F. Dörfler, J. W. Simpson-Porco, and F. Bullo, "Plug-and-play control and optimization in microgrids," in *53rd IEEE Conference on Decision and Control*, Dec 2014, pp. 211–216.

[14] S. Bansal, M. N. Zeilinger, and C. J. Tomlin, "Plug-and-play model predictive control for electric vehicle charging and voltage control in smart grids," in *53rd IEEE Conference on Decision and Control*, Dec 2014, pp. 5894–5900.

[15] S. Lucia, M. Kögel, and R. Findeisen, "Contract-based predictive control of distributed systems with plug and play capabilities," *IFAC-PapersOnLine*, vol. 48, no. 23, pp. 205–211, 2015.

[16] S. Bodenburg and J. Lunze, "Plug-and-play control of interconnected systems with a changing number of subsystems," in *Control Conference (ECC), 2015 European*. IEEE, 2015, pp. 3520–3527.

[17] J. Bendtsen, K. Trangbaek, and J. Stoustrup, "Plug-and-play control—modifying control systems online," *IEEE Transactions on Control Systems Technology*, vol. 21, no. 1, pp. 79–93, 2013.

[18] S. Riverso, M. Farina, and G. Ferrari-Trecate, "Plug-and-Play Decentralized Model Predictive Control for Linear Systems," *IEEE Transactions on Automatic Control*, vol. 58, no. 10, pp. 2608–2614, 2013.

[19] M. Tucci, S. Riverso, and G. Ferrari-Trecate, "Voltage stabilization in DC microgrids through coupling-independent plug-and-play controllers," in *55th Conference on Decision and Control*, 2016, pp. 4944–4949.

[20] J. Schiffer, D. Zonetti, R. Ortega, A. Stankovic, T. Sezi, and J. Raisch, "Modeling of microgrids-from fundamental physics to phasors and voltage sources," 2015. [Online]. Available: arXiv:1505.00136

[21] F. Dörfler and F. Bullo, "Kron reduction of graphs with applications to electrical networks," *IEEE Transactions on Circuits and Systems I: Regular Papers*, vol. 60, no. 1, pp. 150–163, 2013.

[22] M. Tucci, A. Floriduz, S. Riverso, and G. Ferrari-Trecate, "Plug-and-play control of AC islanded microgrids with general topology," in *European Control Conference (ECC)*, 2015, pp. 1493–1500.

[23] S. Riverso, F. Sarzo, and G. Ferrari-Trecate, "Plug-and-play voltage and frequency control of islanded microgrids with meshed topology," Pavia, Italy, Tech. Rep., 2014. [Online]. Available: arXiv:1405.2421

[24] C. Godsil and G. Royle, "Algebraic graph theory, volume 207 of Graduate Texts in Mathematics," 2001.

[25] H. K. Khalil, *Nonlinear systems (3rd edition)*. Prentice Hall, 2001.

[26] IEEE, "IEEE Recommended Practice for Monitoring Electric Power Quality," IEEE Std 1159$^{\text{TM}}$-2009, 3 Park Avenue, New York, NY 10016-5997, USA, 29 June, Tech. Rep. June, 2009.